

APOLLO

GUIDANCE, NAVIGATION AND CONTROL

Approved: A. Kosmala Date: 26 Nov 68
A. KOSMALA, DIRECTOR, SUPPORT PROGRAM DEVEL.
APOLLO GUIDANCE AND NAVIGATION PROGRAM

Approved: G. N. Cherry Date: 26 Nov 68
G. CHERRY, LUMINARY PROJECT MANAGER
APOLLO GUIDANCE AND NAVIGATION PROGRAM

Approved: R. H. Battin Date: 26 Nov 68
R. BATTIN, DIRECTOR, MISSION DEVELOPMENT
APOLLO GUIDANCE AND NAVIGATION PROGRAM

Approved: D. G. Hoag Date: 26 Nov 68
D. G. HOAG, DIRECTOR
APOLLO GUIDANCE AND NAVIGATION PROGRAM

Approved: R. R. Ragan Date: 26 Nov 1968
R. R. RAGAN, DEPUTY DIRECTOR
INSTRUMENTATION LABORATORY

R-567

GUIDANCE SYSTEM OPERATIONS PLAN
FOR MANNED LM EARTH ORBITAL AND
LUNAR MISSIONS USING
PROGRAM LUMINARY

SECTION 6 CONTROL DATA

NOVEMBER 1968

**MIT INSTRUMENTATION
LABORATORY**
CAMBRIDGE 39, MASSACHUSETTS

ACKNOWLEDGEMENT

This report was prepared under DSR Project 55-23870, sponsored by the Manned Spacecraft Center of the National Aeronautics and Space Administration through Contract NAS 9-4065 with the Instrumentation Laboratory, Massachusetts Institute of Technology, Cambridge, Mass.

Principal contributors to the digital simulation data were Herb Chasan and Keith Glick who together prepared the sections on LM and CSM Spacecraft Data. Keith Glick also presented the LM Radar section, new to this revision, and up-dated the Prelaunch from earlier Sunburst data. Herb Chasan revised the Natural Environment data from the Sunburst documentation prepared by William Widnall who also contributed to the earlier Prelaunch data.

The hybrid simulation data were prepared by Philip Felleman and James Cutter.

Editing and copy preparation were supervised by Joseph Glendenning. The text editing programs were written by David Crocker.

R-567

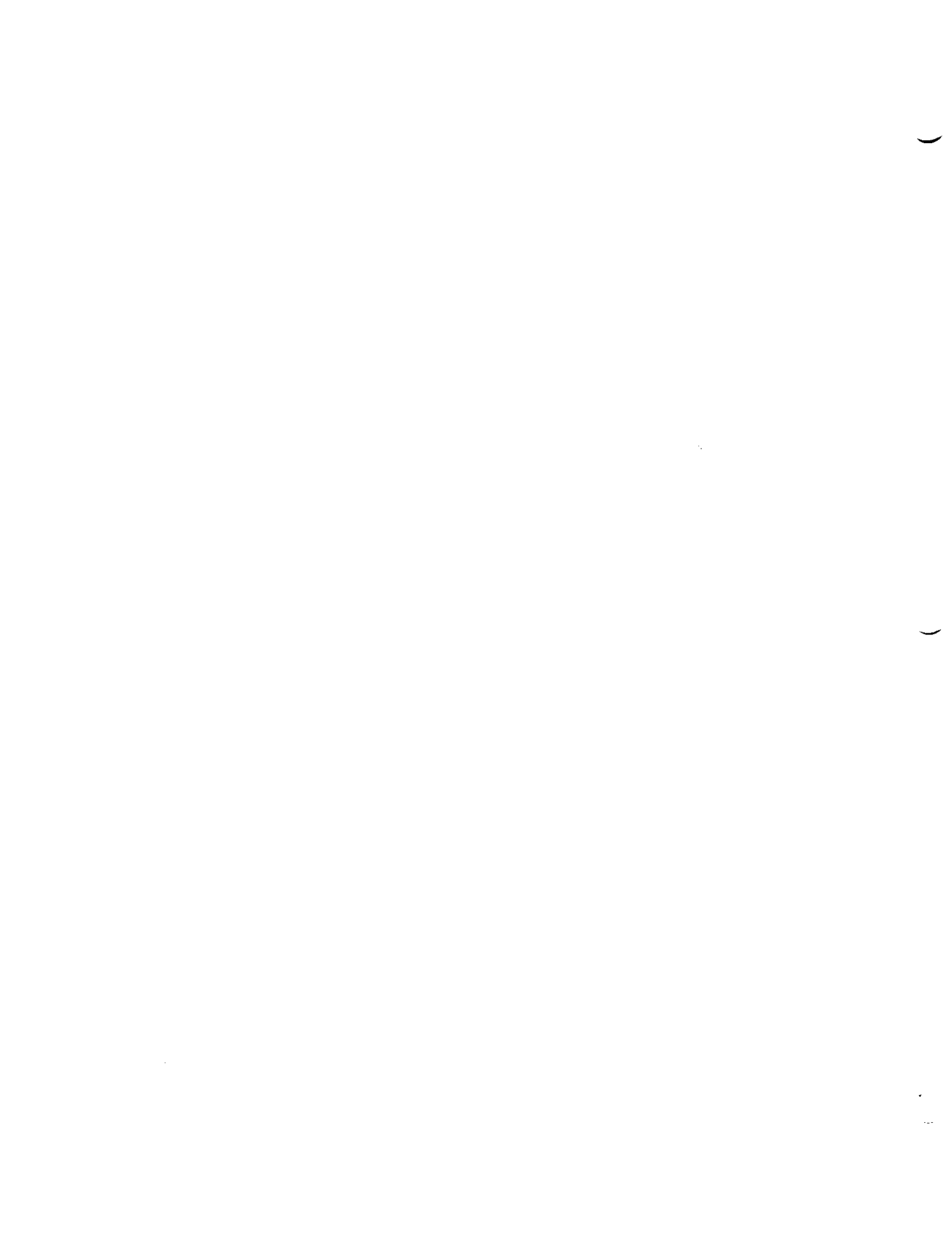
GUIDANCE SYSTEM OPERATIONS PLAN
FOR MANNED LM EARTH ORBITAL AND
LUNAR MISSIONS USING
PROGRAM LUMINARY
SECTION 6 CONTROL DATA

Signatures appearing on this page designate
approval of this document by NASA/MSC.

Approved: _____ Date: _____
Thomas F. Gibson
Asst. Chief, Flight Software Branch
Manned Spacecraft Center, NASA

Approved: _____ Date: _____
James C. Stokes, Jr.
Chief, Flight Software Branch
Manned Spacecraft Center, NASA

Approved: _____ Date: _____
Lynwood C. Dunseith
Chief, Flight Support Division
Manned Spacecraft Center, NASA



6. CONTROL DATA

6.1 Introduction

The Guidance System Operations Plan is published as six separate volumes (sections) as listed below:

Section 1	Prelaunch
Section 2	Data Links
Section 3	Digital Auto-Pilots
Section 4	Operational Modes
Section 5	Guidance Equations
Section 6	Control Data

This volume (Section 6) is published as a summary of data used in the digital and hybrid simulators in support of the verification of the LGC program LUMINARY. The data presented herein represent the most current data available at the time the simulator underwent configuration control. Brief discussions of the most significant mathematical models are included. The data are arranged as follows:

Section 6.2	Digital Simulator Prelaunch Environment Data, describing the gravity and swaying booster simulation used to verify the prelaunch operations.
Section 6.3	Digital Simulator Launch Vehicle Data, not used for this mission program.
Section 6.4	Digital Simulator LM and CSM Spacecraft Data, including reference positions and dimensions, mass properties, propulsion data, and dynamic models for staging forces, propellant slosh effects and structural bending effects.
Section 6.5	Digital Simulator LM Radar Data, including models of landing and rendezvous radar self-test modes, rendezvous radar designate mode and rendezvous radar tracking mode.
Section 6.6	Digital Simulator Coordinate Systems and Natural Environment Data, describing models used which influence the spacecraft trajectory.
Section 6.7	Hybrid Simulator Prelaunch Environment Data, not used for this mission program.
Section 6.8	Hybrid Simulator Launch Vehicle Data, not used for this mission program.
Section 6.9	Hybrid Simulator Spacecraft Data

- Section 6.10 Hybrid Simulator Radar Data
- Section 6.11 Hybrid Simulator Coordinate Systems and Natural Environment Data
- Section 6.12 References, listing the basic source documents from which the control data and models were derived.

In Sections 6.2 through 6.11, a number in the right hand column, opposite a data entry, is the identifying number of the source document as given in the Reference Section 6.12. A more detailed description of the various simulation models used by MIT/IL is given in references 1.1 and 1.2.

This volume constitutes a control document. Revisions to it require NASA approval. Contact H. Chasan (617-864-6900 Ext 1293) or J. O'Connor (Ext 1118) regarding questions or corrections to data in this document.

6.2 Digital Simulator Prelaunch Environment Data

6.2.1 To simulate a prelaunch environment, the position, velocity, gravity and time integral of gravity at the spacecraft navigation base are computed as analytic functions of time, and not by the numerical integration method used in the flight mode.

The gravitational acceleration includes perturbations due to earth oblateness, and sun and moon attractions. The centripetal acceleration due to earth rotation is then added to the gravitational acceleration vector.

Earth rotation rate expressed in the reference coordinate system	WE	0.0 0.0 72921.2×10^{-9}	rad/sec rad/sec rad/sec	2.1
North latitude of the launch site	LAT	28.079	deg	
East longitude of the launch site	LONG	279.43507	deg	
Altitude of the spacecraft navigation base above the reference ellipsoid	ALT	56.7	m	
Spacecraft + Z axis measured counterclockwise from east	AZIMUTH	180	deg	2.2

6.2.2 Superimposed on the deterministic model of gravity and earth rotation is a stochastic model for the launch vehicle swaying in the wind on the launch pad. The swaying motion is assumed to have no preferred direction, so it is modeled by two independent random processes in the two horizontal directions. The swaying booster is modeled as a damped second order oscillator so that the displacement, r , is related to the normalized force, f , by the differential equation

$$\ddot{r} + 2 a w \dot{r} + w^2 r = f$$

Damping ratio of the vehicle for swaying motion		0.1	n/a	2.3
--	--	-----	-----	-----

6.3 Digital Simulator Launch Vehicle Data

Intentionally Blank

Launch vehicle data is not required for the LUMINARY program

6.4 Digital Simulator LM (LM-6) and CSM (CM-107) Spacecraft Data

6.4.1 LM Reference Positions and Tolerances

The following X, Y, and Z coordinates define reference positions in the LM vehicle coordinate system. Tolerances are given in the appropriate units.

The LM vehicle coordinate system is a right hand orthogonal system with its origin fixed at a point 254 inches (6.4516 meters) below the RCS reference plane.

- X is measured up relative to the astronaut
- Y is measured toward the astronaut's right
- Z is measured forward relative to the astronaut

6.4.1.1 LM Descent Engine

Pivot point position	DENG	3.9116	m	4.1
		0.0	m	
		0.0	m	
Three-sigma error	DEPOSERR	±0.00508	m	
tolerance on above		±0.00508	m	
point (DENG)		±0.00508	m	

6.4.1.2 LM Ascent Engine

Point of application	AENG	5.91718	m	4.14
of thrust		0.0	m	
		0.09525	m	
Three-sigma error	AEPOSERR	±0.00762	m	
tolerance on above		±0.00762	m	
point (AENG)		±0.00762	m	

6.4.1.3 LM Navigation Base

Intersection of the three accelerometer input axes	NB		7.79780 m	4.2
			0.0 m	
			1.266825 m	

6.4.1.4 LM Reaction Control System Thruster Positions and Tolerances

Thruster IV-U	Jet 1	RCPOS ₃	6.57352 m	4.1
			1.67894 m	
			1.67894 m	
Thruster IV-D	Jet 2	RCPOS ₆	6.31698 m	
			1.67894 m	
			1.67894 m	
Thruster IV-F	Jet 3	RCPOS ₉	6.4516 m	
			1.5621 m	
			1.68529 m	
Thruster IV-S	Jet 4	RCPOS ₁₂	6.4516 m	
			1.68529 m	
			1.5621 m	
Thruster III-U	Jet 5	RCPOS ₁₅	6.57352 m	
			1.67894 m	
			-1.67894 m	
Thruster III-D	Jet 6	RCPOS ₁₈	6.31698 m	
			1.67894 m	
			-1.67894 m	
Thruster III-F	Jet 7	RCPOS ₂₁	6.4516 m	
			1.5621 m	
			-1.68529 m	
Thruster III-S	Jet 8	RCPOS ₂₄	6.4516 m	
			1.68529 m	
			-1.5621 m	

Thruster II-U	Jet 9	RCPOS ₂₇	6.57352 m
			-1.67894 m
			-1.67894 m
Thruster II-D	Jet 10	RCPOS ₃₀	6.31698 m
			-1.67894 m
			-1.67894 m
Thruster II-F	Jet 11	RCPOS ₃₃	6.4516 m
			-1.5621 m
			-1.68529 m
Thruster II-S	Jet 12	RCPOS ₃₆	6.4516 m
			-1.68529 m
			-1.5621 m
Thruster I-U	Jet 13	RCPOS ₃₉	6.57352 m
			-1.67894 m
			1.67894 m
Thruster I-D	Jet 14	RCPOS ₄₂	6.31698 m
			-1.67894 m
			1.67894 m
Thruster I-F	Jet 15	RCPOS ₄₅	6.4516 m
			-1.5621 m
			1.68529 m
Thruster I-S	Jet 16	RCPOS ₄₈	6.4516 m
			-1.68529 m
			1.5621 m
Three-sigma position error tolerance for each RCS jet		RCPOSERR	±0.00762 m
			±0.00762 m
			±0.00762 m
Three-sigma angular alignment tolerance of each RCS quad about each vehicle axis		RCMISAL	±0.05236 rad

6.4.1.5 LM Propellant Tank Positions

DPS Tank 1 Position	TANKPOS ₃	4.067429 m	4.2
		1.3716 m	
		0.0 m	
DPS Tank 2 Position	TANKPOS ₆	4.067429 m	
		-1.3716 m	
		0.0 m	
DPS Tank 3 Position	TANKPOS ₉	4.067429 m	
		0.0 m	
		1.3716 m	
DPS Tank 4 Position	TANKPOS ₁₂	4.067429 m	
		0.0 m	
		-1.3716 m	
APS Tank 1 Position	TANKPOS ₁₅	5.791403 m	4.2
		-1.8099 m	
		0.0 m	
APS Tank 2 Position	TANKPOS ₁₈	5.791403 m	
		1.1308 m	
		0.0 m	

6.4.2 CSM Reference Positions and Dimensions

The following reference positions and dimensions are expressed in the CSM coordinate system. The relation between CSM and LM vehicle coordinates is given below in terms of the displacement of the LM origin in the CSM system and a transformation matrix which when pre-multiplying a vector in CSM coordinates converts it to LM vehicle coordinates.

Position of LM	X	DISP	36.1378 m	4.30
coordinate origin	Y		0.0 m	
in CSM coordinates	Z		0.0 m	

Transformation matrix from CSM coordinates to LM coordinates	T_{LA}	-1.0 0.0 0.0 0.0 0.5 0.86603 0.0 0.86603 -0.5	nd	
Radius of Service Module (SM) storage oxidizer and fuel tanks	RSTOR	0.5715	m	4.31
X station for geometric center of SM storage oxidizer and fuel tanks	CSTOR	23.1223	m	4.32
Radius of SM sump oxidizer and fuel tanks	RSUMP	0.6477	m	4.31
X station for geometric center of SM sump oxidizer and fuel tanks	CSUMP	23.0861	m	4.32

6.4.3 LM Mass Properties

The LM mass properties are presented at three propellant loadings for both the ascent-descent and the ascent-only configurations. At each propellant loading the initial tanked RCS propellant mass is included (see 6.4.3.3). The inertia for each propellant loading is calculated assuming that the liquid propellant is composed of a rigid mass and a sloshing mass and has no moment of inertia about its own axis (the liquid is assumed to be irrotational). During the simulated mission, adjustments are made to the mass properties as propellant is burned. These are done by parabolic interpolation between the tabulated entries for the DPS and APS propellant loadings. Changes are also made to account for any RCS propellant used. Modifications to the mass properties are made to include the effect of either DPS fuel or oxidizer shifting between its two connected tanks due to the static heads of propellants attempting to remain perpendicular to the engine thrust vector.

In addition to the nominal modifications to the mass properties mentioned above, the center of gravity for the ascent-descent configuration may be effected by a propellant shift due to unbalanced heating of the DPS tanks. This condition, due to either the DPS fuel or the oxidizer shifting between its two connecting tanks, occurs in the absence of an accelerating force and changes the center of gravity at engine ignition (see 6.4.3.4).

Usable propellant loadings depend on the mission objective rather than on the tank capacities (as specified in reference 4.4). If the usable propellant loadings are revised from those cited in 6.4.3.5, it is not necessary to change the LM mass properties at the six propellant loadings. During the simulated mission the center of gravity and the inertia can be corrected for the new propellant loadings after doing the parabolic interpolations.

The inertia matrix is defined as:

$$\begin{aligned}
 I_{XX} &= \int (Y^2 + Z^2) dm & J_{XY} &= - \int XY dm & J_{XZ} &= - \int XZ dm \\
 J_{YX} &= - \int XY dm & I_{YY} &= \int (X^2 + Z^2) dm & J_{YZ} &= - \int YZ dm \\
 J_{ZX} &= - \int XZ dm & J_{ZY} &= - \int YZ dm & I_{ZZ} &= \int (X^2 + Y^2) dm
 \end{aligned}$$

6.4.3.1 Ascent-Descent Configuration

The landing gear is deployed.

Descent Stage			
DPS propellant loading		100% of usable	4.30
Ascent Stage			
APS propellant loading		100% of usable	4.13
Mass		ML ₀	15025.3 kg
Center of Gravity	X	CGL ₀	4.7515 m
	Y		0.0022 m
	Z		0.0183 m

Inertia Values	I_{XX}	IL_0	31222.2	$kg\ m^2$
	J_{XY}		-127.5	$kg\ m^2$
	J_{XZ}		-835.5	$kg\ m^2$
	J_{YX}		-127.5	$kg\ m^2$
	I_{YY}		33931.6	$kg\ m^2$
	J_{YZ}		-369.8	$kg\ m^2$
	J_{ZX}		-835.5	$kg\ m^2$
	J_{ZY}		-369.8	$kg\ m^2$
	I_{ZZ}		33968.8	$kg\ m^2$

Descent Stage

DPS propellant loading 50% of usable

Ascent Stage

APS propellant loading 100% of usable

Mass		ML_1	11036.4	kg
------	--	--------	---------	----

Center of Gravity	X	CGL_3	4.9302	m
	Y		0.0034	m
	Z		0.0254	m

Inertia Values	I_{XX}	IL_9	23725.0	$kg\ m^2$
	J_{XY}		-118.9	$kg\ m^2$
	J_{XZ}		-783.5	$kg\ m^2$
	J_{YX}		-118.9	$kg\ m^2$
	I_{YY}		28258.7	$kg\ m^2$
	J_{YZ}		-364.7	$kg\ m^2$
	J_{ZX}		-783.5	$kg\ m^2$
	J_{ZY}		-364.7	$kg\ m^2$
	I_{ZZ}		30017.5	$kg\ m^2$

Descent Stage

DPS propellant loading 0% of usable

Ascent Stage

APS propellant loading 100% of usable

Mass		ML ₂	7047.5	kg
Center of Gravity	X	CGL ₆	5.5245	m
	Y		0.0059	m
	Z		0.0406	m
Inertia Values	I _{XX}	IL ₁₈	16225.4	kg m ²
	J _{XY}		-91.4	kg m ²
	J _{XZ}		-611.2	kg m ²
	J _{YX}		-91.4	kg m ²
	I _{YY}		16834.0	kg m ²
	J _{YZ}		-359.1	kg m ²
	J _{ZX}		-611.2	kg m ²
	J _{ZY}		-359.1	kg m ²
	I _{ZZ}		20333.9	kg m ²

6.4.3.2 Ascent-Only Configuration

Ascent Stage 4.30
 APS propellant loading 100% of usable 4.13

Mass		ML ₃	4933.3	kg
Center of Gravity	X	CGL ₉	6.2036	m
	Y		0.0026	m
	Z		0.0582	m
Inertia Values	I _{XX}	IL ₂₇	9138.9	kg m ²
	J _{XY}		-38.2	kg m ²
	J _{XZ}		-187.2	kg m ²
	J _{YX}		-38.2	kg m ²
	I _{YY}		4684.6	kg m ²
	J _{YZ}		32.3	kg m ²
	J _{ZX}		-187.2	kg m ²
	J _{ZY}		32.3	kg m ²
	I _{ZZ}		8250.5	kg m ²

Ascent Stage

APS propellant loading

50% of usable

Mass		ML ₄	3781.6	kg
Center of Gravity	X	CGL ₁₂	6.3261	m
	Y		0.0022	m
	Z		0.0760	m
Inertia Values	I _{XX}	IL ₃₆	6795.3	kg m ²
	J _{XY}		-39.2	kg m ²
	J _{XZ}		-152.2	kg m ²
	J _{YX}		-39.2	kg m ²
	I _{YY}		4414.7	kg m ²
	J _{YZ}		32.2	kg m ²
	J _{ZX}		-152.2	kg m ²
	J _{ZY}		32.2	kg m ²
	I _{ZZ}		5648.3	kg m ²

Ascent Stage

APS propellant loading

0% of usable

Mass		ML ₅	2629.9	kg
Center of Gravity	X	CGL ₁₅	6.5588	m
	Y		0.0023	m
	Z		0.1097	m
Inertia Values	I _{XX}	IL ₄₅	4445.3	kg m ²
	J _{XY}		-38.9	kg m ²
	J _{XZ}		-85.4	kg m ²
	J _{YX}		-38.9	kg m ²
	I _{YY}		3921.0	kg m ²
	J _{YZ}		32.2	kg m ²
	J _{ZX}		-85.4	kg m ²
	J _{ZY}		32.2	kg m ²
	I _{ZZ}		2825.2	kg m ²

6.4.3.3 During the simulated mission the vehicle mass properties are adjusted as RCS propellant is used. In the tanks, the usable propellant is assumed to be above the unusable propellant.

RCS propellant			100% of usable		
Mass		TMRFUEL	266.7	kg	4.30
Center of Gravity	X	CGRCS1	7.1018	m	
	Y		0.0	m	
	Z		0.0	m	
Inertia Values	I_{XX}	IRF	367.4	kg m^2	
	J_{XY}		0.0	kg m^2	
	J_{XZ}		0.0	kg m^2	
	J_{YX}		0.0	kg m^2	
	I_{YY}		35.1	kg m^2	
	J_{YZ}		33.0	kg m^2	
	J_{ZX}		0.0	kg m^2	
	J_{ZY}		33.0	kg m^2	
	I_{ZZ}		332.3	kg m^2	
Height of RCS propellant surface above RCS propellant center of gravity		HRCSP	0.3708	m	
Y and Z coordinates of the four RCS tank geometric centers	Y	RTANKPOSY	± 1.13284	m	
	Z	RTANKPOSZ	± 0.3683	m	
RCS Fuel Density		RFDENS	902.3	kg/m^3	
RCS Oxidizer Density		RODENS	1442.5	kg/m^3	

6.4.3.4 In addition to the nominal motion of the center of gravity, a time dependent shift can be included at DPS ignition to model the effect of propellant shift between the descent tanks.

The center of gravity is shifted instantaneously at DPS ignition and thereafter decays to the nominal location exponentially with time measured from DPS ignition. The magnitude of the shift is a function of the DPS propellant load remaining at ignition. It increases linearly from zero for full tanks to a maximum for half-full tanks and then decreases linearly to zero for empty tanks.

Maximum center of gravity shift due to propellant shift	DCGMAX	X	0.1346	m	4.15
		Y	0.2007	m	
		Z	0.3226	m	
Time constant of the center of gravity offset decay	CGTC		50.0	sec	4.16

6.4.3.5 LM Initial Usable Propellant Loads and Densities

DPS usable propellant mass	TMDFUEL		7977.8	kg	4.30
APS usable propellant mass	TMAFUEL		2303.3	kg	
APS usable oxidizer mass	MAOX		1420.5	kg	
APS usable fuel mass	MAF		882.8	kg	
APS or DPS fuel density	FUELDENS		902.3	kg/m ³	
APS or DPS oxidizer density	OXDENS		1442.5	kg/m ³	

6.4.4 CSM Mass Properties

When the LM and CSM are docked and the LM is the controlling vehicle, the mass of the SM propellant is assumed fixed and located at the LM end of its tanks. The center of gravity of the propellant is calculated with the assumption that the SM tanks are cylindrical with the same geometric center and volume as the actual tanks. The inertia of the propellant is calculated with the assumption that the propellant is in the shape of a slender rod with the same mass and height as the actual propellant. These assumptions are also used to find the propellant center of gravity and height in the tank for slosh parameter evaluation. The center of gravity is expressed in the CSM coordinate system. The inertia is given about the center of gravity of each item. See 6.4.3 for the definition of the inertia matrix.

6.4.4.1 Full CSM in orbit less two crewmen with the LM pushing the CSM

Mass		MCSM	27737.6	kg	4.33
Center of Gravity	X	CGCSM	23.986	m	4.33
	Y		0.097	m	
	Z		0.168	m	
Inertia Values	I_{XX}	ICSM	45012.1	kg m^2	
	J_{XY}		2404.1	kg m^2	
	J_{XZ}		-282.4	kg m^2	
	J_{YX}		2404.1	kg m^2	
	I_{YY}		98487.5	kg m^2	
	J_{YZ}		-4263.5	kg m^2	
	J_{ZX}		-282.4	kg m^2	
	J_{ZY}		-4263.5	kg m^2	
	I_{ZZ}		101822.7	kg m^2	

6.4.4.2 SM Propellants

The service module has oxidizer and fuel sump tanks and oxidizer and fuel storage tanks. Propellant is first depleted from the storage tanks and then from the sump tanks.

6.4.4.2.1 SM tanked propellant with the LM pushing the CSM

Mass		TMCFUEL	16978.0	kg	4.33
Center of Gravity	X	CGP	23.313	m	
	Y		0.206	m	
	Z		0.137	m	
Inertia Values	I_{XX}	IP	25575.1	kg m^2	
	J_{XY}		260.3	kg m^2	
	J_{XZ}		-333.0	kg m^2	
	J_{YX}		260.3	kg m^2	
	I_{YY}		25341.2	kg m^2	
	J_{YZ}		-4729.6	kg m^2	
	J_{ZX}		-333.0	kg m^2	
	J_{ZY}		-4729.6	kg m^2	
	I_{ZZ}		30884.5	kg m^2	

6.4.4.2.2 Propellant Densities

SM Fuel Density	CFDENS	902.96	kg/m ³	4.34
SM Oxidizer Density	CODENS	1443.58	kg/m ³	

6.4.4.2.3 Sump tank propellant with the LM pushing the CSM

Mass		MSU	10173.0	kg	4.35
Center of Gravity	X	CGSU	23.180	m	
	Y		0.283	m	
	Z		0.039	m	
Inertia Values	I _{XX}	ISU	14768.6	kg m ²	
	J _{XY}		0.0	kg m ²	
	J _{XZ}		0.0	kg m ²	
	J _{YX}		0.0	kg m ²	
	I _{YY}		10616.28	kg m ²	
	J _{YZ}		-1981.08	kg m ²	
	J _{ZX}		0.0	kg m ²	
	J _{ZY}		-1981.08	kg m ²	
	I _{ZZ}		24843.49	kg m ²	

Sump Tank Oxidizer

Mass		MSUO	6258.8	kg	
Center of Gravity	X	CGSUO	23.180	m	
	Y		1.227	m	
	Z		0.168	m	

Inertia Values	I_{XX}	ISUO	0.0	kg m^2
	J_{XY}		0.0	kg m^2
	J_{XZ}		0.0	kg m^2
	J_{YX}		0.0	kg m^2
	I_{YY}		6365.0	kg m^2
	J_{YZ}		0.0	kg m^2
	J_{ZX}		0.0	kg m^2
	J_{ZY}		0.0	kg m^2
	I_{ZZ}		6365.0	kg m^2

Sump Tank Fuel

Mass		MSUF	3914.2	kg
Center of Gravity	X	CGSUF	23.180	m
	Y		-1.227	m
	Z		-0.168	m
Inertia Values	I_{XX}	ISUF	0.0	kg m^2
	J_{XY}		0.0	kg m^2
	J_{XZ}		0.0	kg m^2
	J_{YX}		0.0	kg m^2
	I_{YY}		3980.5	kg m^2
	J_{YZ}		0.0	kg m^2
	J_{ZX}		0.0	kg m^2
	J_{ZY}		0.0	kg m^2
	I_{ZZ}		3980.5	kg m^2

6.4.4.2.4 Storage tank propellant with the LM pushing the CSM

Mass		MST	6805.0	kg	4.35
Center of Gravity	X	CGST	23.512	m	
	Y		0.091	m	
	Z		0.284	m	

Inertia Values	I_{XX}	IST	10409.5	kg m^2
	J_{XY}		0.0	kg m^2
	J_{XZ}		0.0	kg m^2
	J_{YX}		0.0	kg m^2
	I_{YY}		14028.6	kg m^2
	J_{YZ}		-2941.1	kg m^2
	J_{ZX}		0.0	kg m^2
	J_{ZY}		-2941.1	kg m^2
	I_{ZZ}		5440.5	kg m^2

Storage Tank Oxidizer

Mass		MSTO	4186.4	kg
Center of Gravity	X	CGSTO	23.512	m
	Y		0.376	m
	Z		1.214	m

Inertia Values	I_{XX}	ISTO	0.0	kg m^2
	J_{XY}		0.0	kg m^2
	J_{XZ}		0.0	kg m^2
	J_{YX}		0.0	kg m^2
	I_{YY}		2786.7	kg m^2
	J_{YZ}		0.0	kg m^2
	J_{ZX}		0.0	kg m^2
	J_{ZY}		0.0	kg m^2
	I_{ZZ}		2786.7	kg m^2

Storage Tank Fuel

Mass		MSTF	2618.6	kg
Center of Gravity	X	CGSTF	23.512	m
	Y		-0.376	m
	Z		-1.214	m

Inertia Values	I_{XX}	ISTF	0.0	kg m^2
	J_{XY}		0.0	kg m^2
	J_{XZ}		0.0	kg m^2
	J_{YX}		0.0	kg m^2
	I_{YY}		1743.1	kg m^2
	J_{YZ}		0.0	kg m^2
	J_{ZX}		0.0	kg m^2
	J_{ZY}		0.0	kg m^2
	I_{ZZ}		1743.1	kg m^2

6.4.5 LM Reaction Control System Data

6.4.5.1 The individual RCS thruster is modeled as a constant thrust engine. The buildup and tailoff of thrust are modeled by instantaneous changes in thrust, shifted in time from the electrical command. The shift is different for the application and removal of thrust. The amount of the shift is calculated to give a transient impulse typical of a real thruster.

Step delay in RCS thrust application from receipt of electrical command	RCONDEL	0.019	sec	4.5
Step delay in RCS thrust removal from removal of electrical command	RCOFFDEL	0.015	sec	4.39
Minimum allowed RCS electrical pulse length	TMINPULS	0.013	sec	4.1

The propellant usage of each RCS thruster is given by 4.39

$$\text{FUEL} = \text{TRCON JSECTOKG} + \text{NFIRE NFIRTOKG}$$

FUEL is the mass of propellant used
TRCON is the accumulated firing time of the thruster
NFIRE is the number of firings of the thruster

Constant RCS mass flow rate	JSECTOKG	0.1610	kg/sec
-----------------------------	----------	--------	-----------------

Propellant penalty per firing NFIRTOKG 0.0009525kg

6.4.5.2 The nominal force applied to the vehicle by individual RCS thrusters, expressed in the LM vehicle coordinate system is given below.

Thruster IV-U	Jet 1	RCFORCE ₃	-444.82	n	4.1
			0.0	n	
			0.0	n	
Thruster IV-D	Jet 2	RCFORCE ₆	444.82	n	
			0.0	n	
			0.0	n	
Thruster IV-F	Jet 3	RCFORCE ₉	0.0	n	
			0.0	n	
			-444.82	n	
Thruster IV-S	Jet 4	RCFORCE ₁₂	0.0	n	
			-444.82	n	
			0.0	n	
Thruster III-U	Jet 5	RCFORCE ₁₅	-444.82	n	
			0.0	n	
			0.0	n	
Thruster III-D	Jet 6	RCFORCE ₁₈	444.82	n	
			0.0	n	
			0.0	n	
Thruster III-F	Jet 7	RCFORCE ₂₁	0.0	n	
			0.0	n	
			444.82	n	
Thruster III-S	Jet 8	RCFORCE ₂₄	0.0	n	
			-444.82	n	
			0.0	n	

Thruster II-U	Jet 9	RCFORCE ₂₇	-444.82	n
			0.0	n
			0.0	n
Thruster II-D	Jet 10	RCFORCE ₃₀	444.82	n
			0.0	n
			0.0	n
Thruster II-F	Jet 11	RCFORCE ₃₃	0.0	n
			0.0	n
			444.82	n
Thruster II-S	Jet 12	RCFORCE ₃₆	0.0	n
			444.82	n
			0.0	n
Thruster I-U	Jet 13	RCFORCE ₃₉	-444.82	n
			0.0	n
			0.0	n
Thruster I-D	Jet 14	RCFORCE ₄₂	444.82	n
			0.0	n
			0.0	n
Thruster I-F	Jet 15	RCFORCE ₄₅	0.0	n
			0.0	n
			-444.82	n
Thruster I-S	Jet 16	RCFORCE ₄₈	0.0	n
			444.82	n
			0.0	n

6.4.5.3 With the ascent-descent configuration, the plumes of the +X translation jets impinge on the descent structure. The force each of these jets apply to the vehicle is given below. The force is expressed in the LM vehicle coordinate system.

Thruster IV-D	Jet 2	X	-35.586	n	4.6
		Y	-28.308	n	
		Z	-28.308	n	

Thruster III-D	Jet 6	X	-35.586	n
		Y	-28.308	n
		Z	28.308	n
Thruster II-D	Jet 10	X	-165.474	n
		Y	33.341	n
		Z	33.341	n
Thruster I-D	Jet 14	X	-35.586	n
		Y	28.308	n
		Z	-28.308	n

6.4.5.4 The torque applied about the origin of the GAEC-FMES coordinate system by the impinging plume of each jet is given below. The GAEC-FMES coordinate system has its axes parallel to the respective LM vehicle axes and its origin is given below.

Origin of the GAEC-FMES system in LM coordinates	FMESRP		6.4516	m	4.3
			0.0	m	
			0.0	m	
Thruster IV-D	Jet 2	X	0.0	n m	4.6
		Y	-111.663	n m	
		Z	111.663	n m	
Thruster III-D	Jet 6	X	0.0	n m	
		Y	111.663	n m	
		Z	111.663	n m	
Thruster II-D	Jet 10	X	0.0	n m	
		Y	297.612	n m	
		Z	-297.612	n m	
Thruster I-D	Jet 14	X	0.0	n m	
		Y	-111.663	n m	
		Z	-111.663	n m	

6.4.6 LM Descent Propulsion System Data

6.4.6.1 The DPS thrust buildup and decay upon receipt of the electrical ON-OFF commands are modeled by time delays followed by an instantaneous change in thrust. These delays are calculated to provide transient impulses typical of the real engine. At full throttle the simulated thrust increases linearly with time to model the effect of nozzle and valve erosion. The specific impulse of the DPS is a tabulated function of DPS thrust. At each thrust level a linear interpolation is made between the ISP table entries.

Step delay from LGC engine ON command to application of minimum DPS thrust	DEONDEL	2.55	sec	4.19, 4.38
Step delay from LGC removal of engine ON command to removal of thrust	DEOFFDEL	0.38	sec	4.40
The minimum DPS thrust	FMIN	5337.9	n	4.38
The maximum DPS thrust	FMAX	46706.33	n	4.1
The uneroded maximum DPS thrust	FCMAX	43203.3	n	4.38
Thrust tolerance on FCMAX	FCMAXTOL	±155.7	n	4.18
Thrust tolerance on the DPS thrust at the end of a 370 sec. burn if the burn starts at FCMAX	FENDTOL	±444.8	n	

Specific impulse of the DPS as a function of normalized thrust is given below. The ISP values have the effect of erosion included. The ISP corresponding to a normalized thrust of unity is included to model the decrease in ISP with engine burn time.

	THRUST/FMAX	ISP		
	.114	289.7	sec	4.38
	.115	292.7	sec	
	.252	293.6	sec	
	.401	295.0	sec	
	.925	303.0	sec	
	.945	299.0	sec	

6.4.6.2 The response of the descent engine control assembly to automatic throttle incrementing and decrementing pulses is modeled as a perfect integrator, limited by three non-linearities. The automatic throttle cannot command a thrust level which is less than the minimum thrust level given above. This minimum thrust command corresponds to the ground state or zero of the automatic throttle counter. The automatic throttle is held in this ground state when the DPS is not armed.

Voltage applied to the throttle valve actuator when automatic throttle is in its ground state	VMIN	2.5	v	4.38
---	------	-----	---	------

The LM Guidance Computer (LGC) issues throttle incrementing or decrementing pulses (bits) to an automatic throttle counter whose output goes to a digital-to-analog converter, thus producing a voltage. When the sum of the voltages produced by the throttle digital-to-analog converter and the manual throttle commands the engine to produce its maximum uneroded thrust, additional automatic throttle incrementing commands have no effect.

Voltage which commands maximum uneroded thrust	VMAX	13.8	v	4.17
--	------	------	---	------

The final non-linearity associated with the automatic throttle is the saturation of the automatic throttle counter.

Maximum automatic throttle count		3428	bits	4.15
Rate at which the LGC issues automatic throttle pulses (bits)		3200	bits/sec	4.8, 4.15

Voltage applied to the throttle valve actuator per automatic throttle bit	BTV	0.0035	v/bit	4.15
Thrust command per volt applied to throttle valve actuator	VTN	3645.	n/v	4.38

The thrust response of the descent engine to throttle commands is modeled by a first order lag.

Time constant of thrust response to throttle commands	WDENG	0.3	sec	4.1
Rate of change of thrust at full thrust command to simulate erosion effects	DTD	2.525	n/sec	4.38

6.4.6.3. The orientation of the DPS thrust vector with respect to the LM vehicle coordinate system is determined by the position of the DPS trim gimbals, the fixed misalignment of the engine center line with respect to the vehicle center line, the fixed misalignment of the thrust center line with respect to the engine center line and the thrust dependent misalignment of the thrust vector due to flexing of the mount.

The trim gimbal actuators are modeled as constant speed drives with a time delay in coming to speed and coming to a stop.

Trim gimbal rate	GIMRATE	0.00349	rad/sec	4.1
Trim gimbal drive step ON-OFF delay	TRIMDEL	0.1	sec	
Trim gimbal excursion limits	LMY,LMZ	0.10472	rad	
Time delay from gimbal failure to LGC receipt of a failure signal	GIMFLDEL	0.429	sec	4.22

Three-sigma angular alignment tolerance of the engine center line with respect to the vehicle center line about the noted axes	DEMACL	Y ± 0.005236 rad Z ± 0.005236 rad	4.1
Three-sigma angular alignment tolerance of the thrust center line with respect to the engine center line about the noted axes	DEMATA	Y ± 0.008727 rad Z ± 0.008727 rad	
Thrust dependent misalignment of the thrust center line with respect to the vehicle center line at full thrust about the noted axes	DEMAC	Y $+0.01107$ rad Z -0.01107 rad	4.9

6.4.7 LM Ascent Propulsion System Data

6.4.7.1 The APS thrust buildup and decay upon receipt of the electrical ON-OFF commands are modeled by pure delays followed by an instantaneous change in thrust. These delays are calculated to provide transient impulses typical of the real engine. The thrust of the simulated APS increases linearly with time to model the effect of nozzle and valve erosion. The specific impulse of the APS is a constant.

Step delay from LGC engine ON command to application of thrust (FASCENTN)	AEONDEL	0.382 sec	4.38
Step delay from LGC removal of engine ON command to removal of thrust	AEOFFDEL	0.10 sec	4.40
Uneroded thrust of the APS engine	FASCENTN	15568.8 n	4.41
Specific impulse of the APS	ISPA	309.0 sec	

Rate of change of thrust after the uneroded thrust (FASCENTN) has been attained	DTA	0.0	n/sec	4.15
---	-----	-----	-------	------

Tolerance on the APS thrust at the start of the mission duty cycle		±389.2	n	4.1
--	--	--------	---	-----

Tolerance on the APS thrust at the end of the mission duty cycle		+1089.8	n	
		-389.2	n	

The orientation of the APS engine center line is found by applying the given right hand rotation (IPAY) about the vehicle + Y axis to a vector which is parallel to the vehicle X axis and passes through the point of application of thrust (see 6.4.1.2).

Right hand rotation of APS engine center line	IPAY	-0.02618	rad	4.14
--	------	----------	-----	------

Three-sigma tolerance on the alignment of the thrust center line with respect to the engine center line about the noted axes	AEMISAL	Y ±0.00873	rad	4.14
		Z ±0.00873	rad	

6.4.8 LM Ascent-Descent Staging

The sequencing of events following an abort stage command is determined by two time delays.

Delay from receipt of abort stage command to mechanical separation of stages	STDEL	0.447	sec	4.10
--	-------	-------	-----	------

Delay from receipt of abort stage command to ascent engine thrust buildup to 90% of full rated thrust		0.687	sec	
--	--	-------	-----	--

At APS thrust application, 0.687 seconds after the abort stage command, staging forces and torques are included. These are modeled by two sets of polynomial time series. The first of these model the staging force during the interval immediately following APS ignition, the second set is used after this initial buildup. The staging forces are zeroed at the end of the second interval.

The staging force is given by

$$F_{\text{staging}} = (F_X, F_Y, F_Z) \quad \text{in newtons}$$

The staging torque is given by

$$M_{\text{staging}} = (0, M_Y, M_Z) \quad \text{in newton meters}$$

Where for $t_{\text{ignition}} \leq t \leq t_{\text{ignition}} + 0.10$ 4.11

$$I = [A(t - t_{\text{ignition}})^2 + B(t - t_{\text{ignition}})] 10^5$$

$I = F_X$	$A = -7.11715$	$B = 3.73651$
$I = F_Y$	$A = 0.13345$	$B = 0.08007$
$I = F_Z$	$A = 0.44482$	$B = 0.31138$
$I = M_Y$	$A = 1.95238$	$B = -0.23862$
$I = M_Z$	$A = 14.64283$	$B = -0.24405$

When $(t_{\text{ignition}} + 0.10) \leq t \leq (t_{\text{ignition}} + 0.35)$

$$I = (C(t - t_{\text{ignition}} - 0.10)^2 + D(t - t_{\text{ignition}} - 0.10) + E) 10^5$$

$I = F_X$	$C = 1.99280$	$D = -1.70812$	$E = 0.30248$
$I = F_Y$	$C = 0.10676$	$D = -0.06405$	$E = 0.00934$
$I = F_Z$	$C = 0.39856$	$D = -0.24020$	$E = 0.03559$
$I = M_Y$	$C = 0.20880$	$D = -0.03471$	$E = -0.00434$
$I = M_Z$	$C = 3.05059$	$D = -1.25006$	$E = 0.12202$

The sequencing of events following a lunar launch is as follows. At APS thrust application, AEONDEL seconds after the LGC engine on command, Fire-in-the-Hole forces and torques are included. These are modeled by two sets of polynomial time series. The first of these model the staging force during the interval immediately following APS ignition, the second set is used after this initial buildup. The staging forces are zeroed at the end of the second interval.

The staging force is given by

$$F_{\text{staging}} = (F_X, F_Y, F_Z) \quad \text{in newtons}$$

The staging torque is given by

$$M_{\text{staging}} = (0, M_Y, M_Z) \quad \text{in newton meters}$$

Where for $t_{\text{ignition}} \leq t \leq t_{\text{ignition}} + 0.14$ 4.11

$$I = [A (t - t_{\text{ignition}})^2 + B(t - t_{\text{ignition}})] 10^5$$

$I = F_X$	$A = 12.935$	$B = 0.698$
$I = F_Y$	$A = 0.338$	$B = 0.027$
$I = F_Z$	$A = 2.042$	$B = 0.013$
$I = M_Y$	$A = 0.270$	$B = -0.068$
$I = M_Z$	$A = 9.342$	$B = -0.484$

When $(t_{\text{ignition}} + 0.14) \leq t \leq (t_{\text{ignition}} + 0.64)$

$$I = (C(t - t_{\text{ignition}} - 0.14)^2 + D(t - t_{\text{ignition}} - 0.14) + E) 10^5$$

$I = F_X$	$C = 0.632$	$D = -1.019$	$E = 0.351$
$I = F_Y$	$C = 0.016$	$D = -0.029$	$E = 0.011$
$I = F_Z$	$C = 0.119$	$D = -0.143$	$E = 0.042$
$I = M_Y$	$C = 0.030$	$D = 0.004$	$E = -0.004$
$I = M_Z$	$C = 0.654$	$D = -0.557$	$E = 0.115$

6.4.9 LM Propellant Slosh Model

The effect of propellant sloshing in the LM tanks is modeled by a two dimensional mass-spring oscillator analog for each propellant tank; RCS tanks are neglected. The slosh mass, frequency and attachment points are stored as tabulated functions of the fraction of propellant remaining in the appropriate tank.

The slosh frequency is given by

$$w = \text{LAMBDA} (A_X / R_{\text{tank}})^{1/2} \quad 4.13$$

Where LAMBDA is a function of the liquid level in the tank,

A_X is the contact acceleration along the vehicle X axis and

R_{tank} is the radius of the tank in question.

The following table of slosh parameters is used for the DPS tanks. The slosh masses are expressed in kilograms; the slosh frequency parameter, LAMBDA, in radians. The attachment point is the displacement of the slosh oscillator attachment point, in meters, along the + X vehicle axis measured from the tank geometric center. A linear interpolation is made between tabulated points. The slosh damping is a constant for all tank loadings greater than 2 percent of the total usable propellant. When 2 percent or less of the usable propellant remains, the slosh damping ratio is changed and then held constant to propellant depletion.

Slosh damping ratio when tank loading is greater than 2 percent	SDELC	0.005	1/sec	2.3
Slosh damping ratio when tank loading is less than 2 percent	SDELC	0.1	1/sec	

Fraction of Fuel Remaining	Oxidizer Slosh Mass	Fuel Slosh Mass	LAMBDA	Attachment Point	4.38
0.0	0.0	0.0	1.00	-0.246	
0.1	199.4	125.1	1.09	-0.246	
0.2	373.8	234.6	1.16	-0.246	
0.3	461.0	289.3	1.23	-0.227	
0.4	498.4	312.8	1.29	-0.200	
0.5	523.4	328.4	1.33	-0.155	
0.6	535.8	336.2	1.35	-0.071	
0.7	535.8	336.2	1.38	0.039	
0.8	498.4	312.8	1.44	0.155	
0.9	398.8	250.2	1.56	0.226	
1.0	0.0	0.0	2.50	0.246	

DPS propellant tank radius $TANKR_0$ 0.6477 m 4.30

The following table of slosh parameters is used for the APS tanks.

Fraction of Fuel Remaining	Oxidizer Slosh Mass	Fuel Slosh Mass	LAMBDA	Attachment Point	4.38
0.0	0.0	0.0	1.00	0.0	
0.1	115.3	72.4	1.06	0.0	
0.2	230.5	144.9	1.10	0.0	
0.3	317.0	199.2	1.14	0.0	
0.4	389.0	244.4	1.18	0.0	
0.5	432.2	271.6	1.22	0.0	
0.6	446.6	280.7	1.27	0.0	
0.7	439.4	276.1	1.33	0.0	
0.8	389.0	244.4	1.43	0.0	
0.9	273.7	172.0	1.64	0.0	
1.0	0.0	0.0	2.30	0.0	

APS propellant tank radius $TANKR_1$ 0.62738 m 4.30

6.4.10 CSM Propellant Slosh Model

4.31

The effect of propellant sloshing in the CSM tanks is modeled by a two dimensional mass-spring oscillator analog for each propellant tank; RCS tanks are neglected. The slosh mass, frequency, and attachment point are all calculated using the following relations.

The slosh frequency is given by

$$w = \text{SLFP} (A_X / R_{\text{tank}})^{1/2}$$

where w is the slosh frequency,

A_X is the contact acceleration along the vehicle X axis.

R_{tank} is the radius of the tank in question.

$$\text{SLFP} = (\text{XI} \tanh(\text{XI} \text{HP} / R_{\text{tank}}))^{1/2}$$

$\text{XI} = 1.84$ (argument of Bessel function of the first kind of order one when its derivative is zero)

HP is height of propellant in tank (see 6.4.4)

\tanh is hyperbolic tangent

The slosh mass is given by

$$\text{SM} = \text{MP} \frac{2 \tanh(\text{XI} \text{HP} / R_{\text{tank}})}{[(\text{XI}^2 - 1) \text{XI} \text{HP} / R_{\text{tank}}]}$$

where SM is the slosh mass.

MP is the mass of propellant in a tank.

The slosh attachment point is given by

$$\text{SAP} = (\text{CG}_X - \text{HO}, \text{CG}_Y, \text{CG}_Z)$$

\bar{SAP} is the position of the slosh attachment point in CSM coordinates.

(CG_X, CG_Y, CG_Z) is the center of gravity of the propellant in the tanks (See 6.4.4).

$$HO = (HP/2) - (2R_{\text{tank}}/XI) \tanh(XI HP/2R_{\text{tank}})$$

The slosh damping ratio for the CSM propellant tanks is a constant.

Slosh damping ratio for CSM oxidizer tanks	ZETAO	0.005	1/sec	2.3
--	-------	-------	-------	-----

Slosh damping ratio for CSM fuel tanks	ZETA F	0.005	1/sec	2.3
--	--------	-------	-------	-----

6.4.11 CSM/LM Bending

It is necessary to simulate the structural deflections of the spacecraft caused by external loadings or contact forces such as main propulsion system thrust, RCS thrust and fuel slosh. These structural deflections influence the spacecraft control systems by deflecting the navigation base. The bending deflection of the spacecraft can be expanded in terms of an infinite number of orthogonal eigenfunctions or modes and their associated eigenvalues or frequencies. The modes corresponding to the three lowest frequencies are simulated. The external excitations or forcing functions driving these modes can also be expanded in terms of the same eigenfunctions. Since all of the excitations are modeled by forces applied at a point, they are all spatial impulses. The expansion of the driving functions thus becomes the vector inner product of the external force and the normalized deflection of the mode at the point of application of the force. The equation for the generalized coordinate for a given bending mode with the driving terms included is

$$D^2QB_J/DT^2 = - 2 ZETAB_J WB_J D QB_J/DT - WB_J^2 QB_J + \sum_I (DISP_I / GM) \cdot FORCE_I$$

where QB_J is the generalized coordinate associated with the Jth mode,

$ZETAB_J$ is the damping ratio associated with the Jth mode,

WB_J is the frequency associated with the Jth mode,

\bar{FORCE}_I is one of the contact forces which excite the generalized bending coordinates

\bar{DISP}_I is the vector displacement of the point of application of \bar{FORCE}_I ,

GM is the generalized mass associated with the Jth mode.

It is seen that the bending coordinate for each of the three simulated modes is the solution of a second order differential equation.

The motion of the navigation base is the product of the modal displacements at the navigation base and the appropriate derivative of the generalized bending coordinate. For example, the translational velocity of the navigation base due to the Jth bending mode is given by

$$\bar{V}_J = \bar{DISP}_{NB_J} D \bar{Q}B_J / DT$$

where \bar{DISP}_{NB_J} is the modal displacement of the navigation base due to the Jth bending mode.

Similarly rotational displacement of the navigation base is the product of a modal rotation vector at the navigation base and the generalized bending coordinate

$$\bar{\theta} = \bar{SLOP}_{NB_J} \bar{Q}B_J$$

where \bar{SLOP}_{NB_J} is the modal rotation of the navigation base due to the Jth bending mode.

The mode shapes or specifically the displacements and rotations at individual spacecraft stations and the corresponding modal frequencies, depend on the mass distribution of the spacecraft. Data is thus required for representative loading conditions. The data is the displacements and rotations at all points of interest given below, the generalized mass, and the frequency and damping ratio for each mode. Three complete sets of data are given, one for each reference vehicle mass. A linear interpolation based on instantaneous

total vehicle mass is used to obtain the bending parameters at points between two adjacent reference masses. Within a set of data for a given reference mass, each parameter has three entries for a scalar parameter, or nine entries for a vector parameter. The first entry for a scalar parameter, or the first three entries for a vector parameter pertain to the first mode simulated; the second or second three pertain to the second mode simulated; and similarly for the third mode. The vector parameters are expressed in the LM vehicle coordinate system.

6.4.11.1 Bending Data

The following data is expressed in the LM vehicle coordinate system.

Reference spacecraft mass	MB_0	29898.5	kg	4.36
SPS propellant loading	25%			
DPS propellant loading	100%			
APS propellant loading	100%			
Generalized mass used for all modes	GM	175.127	kg	4.36
Frequency of each mode	WB_0	14.074	rad/sec	4.36
		14.954		
		18.661		
Damping ratio for generalized coordinate	$ZETAB_0$	0.005	n d	2.3
		0.005		
		0.005		
Displacement of the DPS trim gimbal station	$DISPGIMB_0$	0.00212	m/m	4.36,
		0.03943		4.37
		0.00043		
		-0.00118		
		0.00035		
		0.04005		
		0.00030		
		0.00049		
		0.00412		

Rotation of the DPS trim gimbal station	SLOPGIMB ₀	0.0	rad/m	
		-0.00101		
		-0.04938		
			0.0	
			0.05087	
			0.00063	
			0.0	
			0.00266	
			-0.00299	
Displacement of DPS fuel tank 1	DISPTANK ₀	0.07252	m/m	
		0.04314		
		-0.00183		
			0.00002	
			-0.00029	
			0.03931	
			0.00901	
			0.00017	
			0.08627	
Displacement of DPS fuel tank 2	DISPTANK ₉	-0.06787	m/m	
		0.04333		
		0.00352		
			0.00198	
			0.00203	
			0.05103	
			-0.00737	
			0.00052	
			-0.07599	

Displacement of DPS oxidizer tank 3 DISPTANK₁₈ 0.00127 m/m
0.04791
0.00158

0.06711
0.00599
0.04649

0.00463
-0.07833
0.00584

Displacement of DPS oxidizer tank 4 DISPTANK₂₇ 0.00255 m/m
0.04182
0.00032

-0.07199
-0.00543
0.04563

-0.00454
0.08674
0.00488

Displacement of APS fuel tank 5 DISPTANK₃₆ -0.08535 m/m
-0.04731
0.0

-0.00246
0.00278
-0.04880

-0.00080
-0.00684
-0.09251

Displacement of APS oxidizer tank 6	DISPTANK ₄₅	0.05247	m/m
		-0.04967	
		-0.00497	
		0.00078	
		0.00023	
		-0.05601	
		-0.00335	
		-0.01188	
		0.03424	

Displacement of SM oxidizer sump tank	DISPTANK ₅₄	0.0	m/m
		0.02502	
		-0.00156	
		0.0	
		-0.00911	
		0.03209	
		0.0	
		0.07548	
		-0.05255	

Displacement of SM fuel sump tank	DISPTANK ₆₃	0.0	m/m
		0.03005	
		-0.00545	
		0.0	
		0.00390	
		0.02126	
		0.0	
		-0.07778	
		0.07292	

Displacement of LM RCS Quad I	DNQUAD ₀	-0.06375	m/m
		-0.06423	
		0.01489	
		0.06980	
		0.00193	
		-0.07815	
		0.01031	
		-0.05548	
		-0.05120	
Displacement of LM RCS Quad II	DNQUAD ₉	-0.05281	m/m
		-0.09003	
		0.01489	
		-0.06281	
		-0.00242	
		-0.07815	
		0.01053	
		0.03624	
		-0.05120	
Displacement of LM RCS Quad III	DNQUAD ₁₈	0.07246	m/m
		-0.09003	
		-0.01090	
		-0.06435	
		-0.00242	
		-0.08250	
		-0.00521	
		0.03624	
		0.04052	

Displacement of LM RCS Quad IV	DNQUAD ₂₇	0.06152	m/m
		-0.06423	
		-0.01090	
		0.06826	
		0.00193	
		-0.08250	
		-0.00543	
		-0.05548	
		0.04052	
Displacement of LM navigation base	DISPNB ₀	-0.00668	m/m
		-0.12383	
		0.00671	
		0.06020	
		0.00510	
		-0.12018	
		0.00411	
		-0.03270	
		-0.01610	
Rotation of LM nav- igation base	SLOPNB ₀	0.01032	rad/m
		-0.00787	
		-0.01673	
		-0.00421	
		0.04972	
		0.00102	
		0.03236	
		0.00476	
		-0.00465	

Reference spacecraft mass	MB_0	25633.4	kg	4.36
SPS propellant loading 25%				
DPS propellant loading 50%				
APS propellant loading 100%				
Generalized mass used for all modes	GM	175.127	kg	4.36
Frequency of each mode	WB_0	12.818	rad/sec	4.36
		12.818		
		18.661		
Damping ratio for generalized coordinate	$ZETAB_0$	0.005	nd	2.3
		0.005		
		0.005		
Displacement of the DPS trim gimbal station	$DISPGIMB_0$	0.0	m/m	4.36
		0.0485		4.37
		0.0		
		0.0		
		0.0		
		0.0485		
		0.0		
		0.0		
		0.0		

Rotation of the DPS trim gimbal station	SLOPGIMB ₀	0.0	rad/m
		0.0	
		-0.06260	
		0.0	
		0.06260	
		0.0	
		0.04331	
		0.0	
		0.0	
		0.0	
Displacement of DPS fuel tank 1	DISPTANK ₀	0.0	m/m
		-0.01850	
		0.0	
		0.0	
		0.0	
		-0.01850	
		0.0	
		0.0	
		0.05940	
		0.0	
Displacement of DPS fuel tank 2	DISPTANK ₉	0.0	m/m
		-0.01850	
		0.0	
		0.0	
		0.0	
		-0.01850	
		0.0	
		0.0	
		-0.05940	
		0.0	

Displacement of DPS oxidizer tank 3 DISPTANK₁₈ 0.0 m/m
-0.01850

0.0

0.0

0.0

-0.01850

0.0

-0.05940

0.0

Displacement of DPS oxidizer tank 4 DISPTANK₂₇ 0.0 m/m
-0.01850

0.0

0.0

0.0

-0.01850

0.0

0.05940

0.0

Displacement of APS fuel tank 5 DISPTANK₃₆ 0.0 m/m
-0.07520

0.0

0.0

0.0

-0.07520

0.0

0.0

-0.07840

Displacement of APS oxidizer tank 6	DISPTANK ₄₅	0.0	m/m
		-0.07520	
		0.0	
		0.0	
		0.0	
		-0.07520	
		0.0	
		0.0	
		0.04900	
		0.0	
Displacement of SM oxidizer sump tank	DISPTANK ₅₄	0.0	m/m
		0.07400	
		0.0	
		0.0	
		0.07400	
		0.0	
		0.05390	
		-0.04190	
		0.0	
		0.07400	
Displacement of SM fuel sump tank	DISPTANK ₆₃	0.0	m/m
		0.07400	
		0.0	
		0.0	
		0.0	
		0.07400	
		0.0	
		-0.05390	
		0.04190	
		0.0	

Displacement of LM RCS Quad I	DNQUAD ₀	-0.10200	m/m
		-0.11100	
		0.0	
		0.10200	
		0.0	
		-0.11100	
		0.0	
		-0.07040	
		-0.07040	
		0.0	
Displacement of LM RCS Quad II	DNQUAD ₉	-0.10200	m/m
		-0.11100	
		0.0	
		-0.10200	
		0.0	
		-0.11100	
		0.0	
		0.070400	
		-0.070400	
		0.0	
Displacement of LM RCS Quad III	DNQUAD ₁₈	0.10200	m/m
		-0.11100	
		0.0	
		-0.10200	
		0.0	
		-0.11100	
		0.0	
		0.070400	
		0.070400	
		0.0	

Displacement of LM RCS Quad IV	DNQUAD ₂₇	0.10200	m/m
		-0.11100	
		0.0	
		0.10200	
		0.0	
		-0.11100	
		0.0	
		-0.07040	
		0.07040	
		0.0	
Displacement of LM navigation base	DISPNB ₀	-0.00950	m/m
		-0.19980	
		0.0	
		0.09070	
		0.0	
		-0.19980	
		0.0	
		-0.06270	
		-0.00660	
		0.0	
Rotation of LM navigation base	SLOPNB ₀	0.0	rad/m
		0.0	
		-0.06260	
		0.0	
		0.06260	
		0.0	
		0.04331	
		0.0	
		0.0	
		0.0	

Reference spacecraft mass	MB_0	22248.3	kg	4.36
SPS propellant loading 25%				
DPS propellant loading 0%				
APS propellant loading 100%				
Generalized mass used for all modes	GM	175.127	kg	4.36
Frequency of each mode	WB_0	13.132	rad/sec	4.36
		13.132		
		19.729		
Damping ratio for generalized coordinate	$ZETAB_0$	0.005	nd	2.3
		0.005		
		0.005		
Displacement of the DPS trim gimbal station	$DISGIMB_0$	0.0	m/m	4.36
		0.05680		4.37
		0.0		
		0.0		
		0.0		
		0.05680		
		0.0		
		0.0		
		0.0		

Rotation of the DPS trim gimbal station	SLOPGIMB ₀	0.0	rad/m
		0.0	
		-0.06535	
		0.0	
		0.06535	
		0.0	
		0.05118	
		0.0	
		0.0	
		0.0	
Displacement of DPS fuel tank 1	DISPTANK ₀	0.0	m/m
		0.10410	
		0.0	
		0.0	
		0.0	
		0.10410	
		0.0	
		0.0	
		0.07020	
		0.0	
Displacement of DPS fuel tank 2	DISPTANK ₉	0.0	m/m
		0.10410	
		0.0	
		0.0	
		0.0	
		0.10410	
		0.0	
		0.0	
		-0.07020	
		0.0	

Displacement of DPS oxidizer tank 3	DISPTANK ₁₈	0.0	m/m
		0.10410	
		0.0	
		0.0	
		0.0	
		0.10410	
		0.0	
		-0.07020	
		0.0	
		0.0	
Displacement of DPS oxidizer tank 4	DISPTANK ₂₇	0.0	m/m
		0.10410	
		0.0	
		0.0	
		0.0	
		0.10410	
		0.0	
		0.07020	
		0.0	
		0.0	
Displacement of APS fuel tank 5	DISPTANK ₃₆	0.0	m/m
		-0.06100	
		0.0	
		0.0	
		0.0	
		-0.06100	
		0.0	
		0.0	
		-0.09250	
		0.0	

Displacement of APS oxidizer tank 6	DISPTANK ₄₅	0.0	m/m
		-0.06100	

0.0
0.0
-0.06100

Displacement of SM oxidizer sump tank	DISPTANK ₅₄	0.0	m/m
		0.07300	

0.0
0.0
0.07300

0.0
0.05000
-0.03890

Displacement of SM fuel sump tank	DISPTANK ₆₃	0.0	m/m
		0.07300	

0.0
0.0
0.07300

0.0
-0.05000
0.03890

Displacement of LM RCS Quad I	DNQUAD ₀	-0.10600	m/m
		-0.10920	
		0.0	
		0.10600	
		0.0	
		-0.10920	
		0.0	
		-0.08320	
		-0.08320	
		0.0	
Displacement of LM RCS Quad II	DNQUAD ₉	-0.10600	m/m
		-0.10920	
		0.0	
		-0.10600	
		0.0	
		-0.10920	
		0.0	
		0.08320	
		-0.08320	
		0.0	
Displacement of LM RCS Quad III	DNQUAD ₁₈	0.10600	m/m
		-0.10920	
		0.0	
		-0.10600	
		0.0	
		-0.10920	
		0.0	
		0.08320	
		0.08320	
		0.0	

Displacement of LM RCS Quad IV	DNQUAD ₂₇	0.10600	m/m
		-0.10920	
		0.0	
		0.10600	
		0.0	
		-0.10920	
		0.0	
		-0.08320	
		0.08320	
		0.0	
Displacement of LM navigation base	DISPNB ₀	-0.00990	m/m
		-0.20220	
		0.0	
		0.09450	
		0.0	
		-0.20220	
		0.0	
		-0.74100	
		-0.00780	
		0.0	
Rotation of LM navigation base	SLOPNB ₀	0.0	rad/m
		0.0	
		-0.06535	
		0.0	
		0.06535	
		0.0	
		0.05118	
		0.0	
		0.0	
		0.0	

6.5 Digital Simulator Rendezvous Radar

For verification purposes, the LM radar system has three modes of operation: a self-test mode; a search-designate mode; and a tracking mode.

6.5.1 The self-test mode is initiated by the appropriate setting of the "RADAR TEST" panel switch. This mode substitutes internally generated test signals for the normal return signal. These test signals can be interrogated by the LGC in the usual manner. The contents of the radar shift register at the end of the 80 millisecond read or strobe interval are given below.

Rendezvous radar self-test range count accumulated over an 80 millisecond sample period	TSTRGE	16204	bits	5.1
Rendezvous radar self-test range rate count simulated over an 80 millisecond sample period	TSTRATE	17796	bits	
Landing radar self-test X velocity count accumulated over an 80 millisecond sample period	TSTVX	12672	bits	5.2
Landing radar self-test Y velocity count accumulated over an 80 millisecond sample period	TSTVY	13056	bits	
Landing radar self-test Z velocity count accumulated over an 80 millisecond sample period	TSTVZ	13056	bits	
Landing radar self-test range count accumulated over an 80 millisecond sample period	TSTALT	1536	bits	

6.5.2 The search-designate mode is initiated by placing the "RADAR MODE" switch in the LGC position and issuing the radar CDU error counter enable. In this mode the rendezvous radar antenna stabilization loops are simulated. The antenna is inertially stabilized in two axes by the stabilization loops which hold the mechanical bore sight fixed in the presence of spacecraft motion. These loops are controlled by the LGC through the radar CDU digital-to-analog converters. The output of the D/A converter is interpreted as a rate command to the antenna shaft or trunnion gimbal torquers. The D/A conversion is linear up to a saturation level.

Commanded antenna rate per CDU error counter pulse	.0004709 rad/sec bit 5.3
Saturation of CDU D/A converter	±384 bits

Mechanical stops limit antenna motion, with respect to the vehicle, to the intervals given below.

Antenna Mode I

Shaft coverage

$$- 126^{\circ} < \theta_S < + 60^{\circ}$$

Trunnion coverage

$$- 90^{\circ} < \theta_T < + 70^{\circ}$$

Antenna Mode II

Shaft coverage

$$- 140^{\circ} < \theta_S < - 20^{\circ}$$

Trunnion coverage

$$- 250^{\circ} < \theta_T < - 90^{\circ}$$

where θ_S is the shaft angle measured in a positive right hand sense about the plus Y vehicle axis,

θ_T is the trunnion angle measured in a positive right hand sense about the plus X vehicle axis when θ_S is zero.

Within the above limits, the stabilization loops are simulated by the following differential equations.

$$D^2 W_S / DT^2 = (W_T \tan \theta_T - K_{01}) D W_S / DT \\ + (K_{01} W_T \tan \theta_T - K_{02}) W_S \\ + K_{02} \sec \theta_T (\gamma W_{SC} - W_{SB})$$

$$D^2 W_T / DT^2 = -K_{11} D W_T / DT - K_{12} W_T + K_{12} (W_{TC} - W_{TB})$$

$$D \theta_S / DT = W_T$$

$$D \theta_T / DT = W_S$$

where W_{SB} is the vehicle rate about the shaft axis,
 W_{TB} is the vehicle rate about the trunnion axis,
 W_{SC} is the shaft rate command from the LGC,
 W_{TC} is the trunnion rate command from the LGC.
 γ inverts the shaft command in antenna mode 2.

$$\gamma = 1, \text{ antenna mode I}$$

$$\gamma = -1, \text{ antenna mode II}$$

The constant coefficients in the above equations are chosen so that the response to a step rate command is typical of a real antenna assembly.

Shaft damping coefficient	K_{01}	20	sec^{-1}	5.6
Shaft restoring coefficient	K_{02}	370	sec^{-2}	

Trunnion damping coefficient	K_{11}	20	sec^{-1}
Trunnion restoring coefficient	K_{12}	370	sec^{-2}

6.5.3 The tracking mode is initiated when the radar antenna has been designated so that the angle between the antenna electrical beam center and the line of sight to the transponder is less than a specified angle and the LGC has issued the "SELF-TRACK ENABLE" discrete to the radar.

In general the orientation of the electrical beam center differs from the orientation indicated to the LGC through the CDU analog-to-digital conversion. This results because of misalignments of the electrical and mechanical bore sights, and misalignments of the mechanical bore sight with respect to the resolvers. To simulate these errors, a fixed error is added to the shaft and trunnion angle. The magnitude of these angular bias errors is left optional but typical values used for testing are given below.

Certain other conditions must be satisfied before the tracking mode commences. These also appear below. When all conditions for tracking are satisfied, the "DATA GOOD" discrete is issued to the LGC and the radar drives the stabilization loops so as to align the antenna electrical beam center with the line of sight to the target.

The tracking mode is terminated when any of the tracking conditions are violated.

Maximum angle between antenna electrical beam center and the line of sight to the transponder at which acquisition can occur		0.03491	rad	5.7
--	--	---------	-----	-----

Maximum range at which acquisition and tracking can occur	MAXR	740800	m
---	------	--------	---

Maximum range rate at which acquisition and tracking can occur	RLIMIT	± 1493.52	m/sec
--	--------	---------------	-------

Typical shaft angle bias errors used in testing	E_0	0.010	rad
---	-------	-------	-----

Typical trunnion angle bias errors used in testing	E_1	0.010	rad
--	-------	-------	-----

In the tracking mode the LGC may interrogate the radar for range and range rate information. At ranges below a specified range, the radar scaling of range information changes and accordingly a discrete is set to inform the LGC of this condition. A bias frequency is added to the range rate measurements. The range rate count is added to the count due to this bias for closing range and subtracted from it for opening ranges.

Rendezvous radar range scale factor for high ranges	RANGESC	0.043721214	bits/m 5.7
---	---------	-------------	------------

Rendezvous radar range scale factor for low ranges	RANGESC	0.34976971	bits/m
--	---------	------------	--------

Range threshold at which range scale factor is changed	LOSC	93681.639	m
--	------	-----------	---

Rendezvous radar range rate scale factor	RRATESC	5.226	bit sec/m
--	---------	-------	-----------

Rendezvous radar range rate bias count based on an 80 millisecond counting interval	RRBIAS	17000	bits
---	--------	-------	------

6.6 Digital Simulator Coordinate Systems and Natural Environment Data

6.6.1 Reference Inertial Coordinate System

The reference inertial coordinate system used in verification of Apollo guidance computer programs is defined by the intersection of the mean equatorial plane and the ecliptic at the nearest beginning of the Besselian year. The rectangular coordinates are defined so that the +X axis is along the ascending node of the ecliptic on the equator (the equinox), the + Z axis is along the mean rotational axis of the earth and the Y axis completes the right-handed set.

The origin of the reference system is the center of mass of the earth.

6.6.2 Geodetic Coordinate System

Positions in the earth fixed system are specified by geodetic latitude, referenced to the Fischer ellipsoid of 1960; longitude, measured positive east from the meridian of Greenwich; and altitude, measured above the ellipsoid along the geocentric radius vector.

A cross-section of the Fischer ellipsoid containing the axis of symmetry has the equation

$$(x^2/a^2) + (z^2/b^2) = 1$$

The equatorial radius of the earth	a	6378165.	m	6.1
The flattening of the ellipsoid	$(a-b)/a$	1/298.3	n/a	6.1
The polar radius of the earth	b	6356784.28	m	6.1

6.6.3 Local Horizontal Coordinate System

The system to which spacecraft attitude is referred is the local horizontal coordinate system. It is defined in terms of the spacecraft position and velocity

expressed in the reference inertial coordinate system such that

$$\begin{aligned}\bar{u}_x &= \bar{u}_y \times \bar{u}_z \\ \bar{u}_y &= \frac{\bar{V}_{ref} \times \bar{R}_{ref}}{\left| \bar{V}_{ref} \times \bar{R}_{ref} \right|} \\ \bar{u}_z &= \frac{-\bar{R}_{ref}}{\left| \bar{R}_{ref} \right|}\end{aligned}$$

Starting with the vehicle coordinate axes initially aligned with the local horizontal system, the application of the Euler rotations pitch, yaw, and roll about the Y, Z and X vehicle axes in that order determines the vehicle attitude.

6.6.4 Earth Gravitational Model

The gravitational potential of the earth is assumed to be

$$\begin{aligned}V_e(r,L) &= (MU_e/r) \left(1 + (J/3) \left(r_e/r \right)^2 \left(1 - 3 \sin^2 L \right) \right. \\ &\quad + (H/5) \left(r_e/r \right)^3 \left(3 - 5 \sin^2 L \right) \sin L \\ &\quad \left. + (D/35) \left(r_e/r \right)^4 \left(3 - 30 \sin^2 L + 35 \sin^4 L \right) \right)\end{aligned}$$

where r_e is the equatorial radius of the earth.

The earth's gravitational parameter	MU_e	$3986032. \times 10^8$	m^3/sec^2	6.1
Oblateness coefficients	J	$162345. \times 10^{-8}$	n/a	6.1
	H	$-575. \times 10^{-8}$	n/a	6.1
	D	$7875. \times 10^{-9}$	n/a	6.1

The mass distribution of the earth is assumed symmetric about the rotational axis, hence there is no dependence on longitude in the potential equation.

6.6.5 Sun and Moon Gravitational Models

The acceleration due to the sun and moon is the difference between the gravitational field at the spacecraft and the field at the origin of the coordinate system. The acceleration of the spacecraft due to the earth, sun and moon relative to an inertial system is

$$\bar{a}_v = \bar{g}_e + (MU_s/r_{vs}^3) \bar{r}_{vs} + (MU_m/r_{vm}^3) \bar{r}_{vm}$$

The acceleration of the earth is

$$\bar{a}_e = (MU_s/r_{es}^3) \bar{r}_{es} + (MU_m/r_{em}^3) \bar{r}_{em}$$

Thus the acceleration of the vehicle relative to the center of mass of the earth is

$$\begin{aligned} \bar{a}_{ev} = \bar{g}_e + MU_s((\bar{r}_{vs}/r_{vs}^3) - (\bar{r}_{es}/r_{es}^3)) \\ + MU_m((\bar{r}_{vm}/r_{vm}^3) - (\bar{r}_{em}/r_{em}^3)) \end{aligned}$$

The sun's gravitational parameter	MU_s	$132715445. \times 10^{12}$	m^3/sec^2	6.1
-----------------------------------	--------	-----------------------------	-------------	-----

The moon's gravitational parameter	MU_m	$4902778. \times 10^6$	m^3/sec^2	6.1
------------------------------------	--------	------------------------	-------------	-----

6.7 Hybrid Simulator Prelaunch Environment Data

Intentionally Blank

Prelaunch data is not used by hybrid simulator for LUMINARY program.

6.8 Hybrid Simulator Launch Vehicle Data

Intentionally Blank

Launch vehicle data is not required for LUMINARY program.

6.9 Hybrid Simulator LM(LM-6) Spacecraft Data

6.9.1 LM Reference Positions

The following X,Y,Z coordinates are referenced to the LM vehicle coordinate system.

6.9.1.1 LM Descent Engine

Engine gimbal plane	X_A	3.9116	m	4.1
	Y_A	0.0	m	
	Z_A	0.0	m	

6.9.1.2 LM Ascent Engine

The LM ascent engine thrust application point is located off the +X vehicle axis and the engine is canted so that a vector along the center line of the engine toward the +X spacecraft direction has a component in the -Z direction.

Engine thrust application point	X_A	5.91718	m	4.14
	Y_A	0.0	m	
	Z_A	0.09525	m	
Engine cant angle	THETA	0.02617	rad	

6.9.1.3 LM Navigation Base

Intersection of the three accelerometer input axes	X_A	7.7978	m	4.2
	Y_{NB}	0.0	m	
	Z_{NB}	1.2668	m	

6.9.1.4 LM Reaction Control System

Thrust application point of up and down jets	Y_E	±1.67894	m	4.1
	Z_E	±1.67894	m	
Thrust application point of front and side jets	Y_E	±1.5621	m	
	Z_E	±1.5621	m	
Front and side jet firing plane	X_E	6.4516	m	

6.9.1.5 LM Propellant Tanks

DPS Tank 1 Position	X	4.0674	m	4.2
	Y	1.3716	m	
	Z	0.0	m	
DPS Tank 2 Position	X	4.0674	m	
	Y	-1.3716	m	
	Z	0.0	m	
DPS Tank 3 Position	X	4.0674	m	
	Y	0.0	m	
	Z	1.3716	m	
DPS Tank 4 Position	X	4.0674	m	
	Y	0.0	m	
	Z	-1.3716	m	
APS Oxidizer Position	X	5.7914	m	4.2
	Y	1.1308	m	
	Z	0.0	m	
APS Fuel Position	X	5.7914	m	
	Y	-1.8099	m	
	Z	0.0	m	

6.9.2 LM Mass Properties

The hybrid simulation of the spacecraft mass properties is as follows. The unstaged spacecraft consists of a fully loaded ascent stage and empty descent stage as a single fixed rigid mass. The DPS propellants are represented as rigid and sloshing masses attached at the appropriate points. The inertia reaction forces and torques contributed by the propellant masses are summed with the forces and torques produced on the empty spacecraft. For the staged configuration, the same principle is used, i.e. empty spacecraft and attached propellant masses. The slosh masses are considered to be slightly damped pendulums. The rigid mass is considered to move with the tank. The sum of the slosh mass and rigid mass represents the total propellant mass. During coasting flight (non-thrusting phases) all propellant is considered as rigidly attached to the tanks.

Apparent discrepancies between the Hybrid and Digital mass data reflect differences in the respective mass models rather than the use of different data.

6.9.2.1 Unstaged LM

The unstaged LM consists of a full ascent and empty descent stage. The full ascent stage in the unstaged configuration includes 80% of the RCS propellant, the APS propellant, and men and equipment. The landing gear is deployed.

Mass	M	6892.03	kg	4.4
				4.13
Center of gravity	X_{CG}	5.5193	m	
	Y_{CG}	0.0	m	
	Z_{CG}	0.0	m	
Inertia Values	I_{XX}	15054.7	kg m ²	
	I_{YY}	16444.5	kg m ²	
	I_{ZZ}	16444.5	kg m ²	
	J_{XY}	-198.4	kg m ²	
	J_{XZ}	920.6	kg m ²	
	J_{YZ}	554.3	kg m ²	

6.9.2.2 Staged Configuration

The empty ascent stage of the staged configuration includes men and equipment but no RCS propellant.

Mass	M	2437.7	kg	4.4
				4.13
Center of gravity	X_{CG}	6.5285	m	
	Y_{CG}	-0.0045	m	
	Z_{CG}	0.1279	m	
Inertia Values	I_{XX}	4128.8	kg m ²	
	I_{YY}	3789.9	kg m ²	
	I_{ZZ}	2381.3	kg m ²	
	J_{XY}	77.5	kg m ²	
	J_{XZ}	152.9	kg m ²	
	J_{YZ}	1.0	kg m ²	

6.9.2.3 Propellant Mass Properties

The mass properties of the propellant are computed for each tank based on the properties for a single oxidizer tank and then multiplied by the mixture ratio for the fuel tanks. This allows for propellant shift between descent tanks.

DPS tank radius	RDES	0.6477	m	4.30
DPS cylindrical length	CYL	0.4897	m	
DPS propellant mass (Full tank capacity)	MLFD	8409.375	kg	
DPS usable propellant load	DESFUELMAX	94.45%		
APS tank radius	RASC	0.6274	m	4.30
APS propellant mass (Full tank capacity)	MLFA	2366.5	kg	
APS usable propellant load	ASCFUELMAX	96.69%		

The following table of slosh parameters is used for the DPS tanks. The slosh masses (MS) are expressed in percent of full tank capacity. The distance, HS, of the attachment point of the pendulum representing slosh mass is given from the bottom of the tank parallel to the spacecraft +X axis. The distance, HR, of the center of mass of the rigid propellant is given from the bottom of the tank parallel to the spacecraft +X axis, and the slosh frequency parameter is defined as $\text{OMEGA}^2/\text{UDOT}$, where UDOT is the acceleration along the spacecraft +X axis. A linear interpolation is made between tabulated points.

Fraction of full capacity	MS MLFD	HS (meters)	HR (meters)	$\text{OMEGA}^2/\text{UDOT}$ (1/meters)	
1.0	0.0	1.14	0.89	9.71	4.13
0.9	0.16	1.12	0.79	3.75	
0.75	0.21	0.95	0.74	3.03	
0.3	0.185	0.66	0.66	2.34	
0.15	0.12	0.65	0.65	1.93	
0.0	0.0	0.65	0.65	1.55	

The following table of slosh parameters is for the ascent tanks:

Fraction of full capacity	MS MLFA	OMEGA ² /UDOT (u/meters)	
1.0	0.0	8.49	4.13
0.9	0.20	4.33	
0.75	0.30	3.05	
0.3	0.22	2.10	
0.15	0.12	1.87	
0.0	0.0	1.61	

HS and HR are constant at 0.6274 meter since the tanks are spherical.

6.9.2.4 DPS Propellant Shift

Due to interconnections of the DPS tanks, it is possible for fuel and oxidizer to shift between either tank at various propellant loadings. The maximum shift occurs at 50% loading when one fuel and one oxidizer tank may be full and the other fuel and oxidizer tank empty. The propellant will shift toward equalization in the presence of acceleration with a time constant of 50 seconds.

6.9.3 LM Reaction Control System Data

In the hybrid simulation the Reaction Control System is modeled as having no delay in turn on or shut off. Accordingly it was necessary to use a reduced value of dribble volume to produce an RCS fuel accounting consistent with the digital simulation. Each thruster produces 444.82 newtons of force. No effects due to jet impingement on the descent stage are taken into account.

RCS propellant flow rate	0.1610 kg/sec	4.39
DRIBBLE mass penalty per jet firing	0.0003085 kg	

6.9.4 LM Descent Propulsion System Data

The hybrid simulation represents both the initial and final transient conditions and the steady state response of the DPS engine by a single damped second order system with a natural frequency of 12.5 radians per second and a damping constant of 0.7.

The thrust level of the engine increases with time due to erosion of the throat.

Rate of change of thrust at full thrust command to simulate erosion effects	K_E	2.525	n/sec	4.38
Minimum thrust	T_{MIN}	5337.9	n	4.38
Maximum thrust (uneroded)	T_{MAX}	43203.3	n	4.38

Specific impulse is represented as a linear function of applied thrust for thrust values below 13344.6 newtons and a constant of 302 seconds for thrust levels above 13344.6 newtons.

$$ISP = 22 \times (THRUST/13344.6) + 280$$

The trim gimbal system determines the direction of the descent engine thrust vector. The trim gimbal drive signal is applied to a first order lag with a time constant of 0.0333 second arriving at full speed in 0.1 second.

Gimbal drive rate		0.00349	rad/sec	4.1
Gimbal drive time constant		0.0333	sec	

6.9.5 LM Ascent Propulsion System

The hybrid simulation represents both the initial and final transient conditions and the steady state response of the APS engine by a single damped second order system with a natural frequency of 12.5 radians per second and a damping constant of 0.7.

Thrust (uneroded)	TASC	15568.8	n	4.41
-------------------	------	---------	---	------

6.10 Hybrid Simulation of Radar Data

The Rendezvous Radar is simulated by two voltage-to-frequency converters which accept dc voltages and produce frequencies centered about 150 kHz for range rate and zero for range. These are varied as a function of the input voltage which provides a change in frequency of 1 Hz for a change of 0.065 volt in the range rate channel and 1 Hz/0.0208 volt for range.

Maximum range	RMAX	740800	m	5.7
Minimum range	RMIN	1000	m	
Low scale factor range	RSCF	92970.4	m	
Range accuracy		1%		
Maximum range rate	RDOTMAX	1500	m/s	
Range rate accuracy		1%		
Radar gimbal torquing rate		0.105	rad/sec	

6.12 References

- 1.1 Digital Simulation for the Verification of Program SUNBURST (Unmanned LM, AS-206), Massachusetts Institute of Technology, Instrumentation Laboratory, E-2146, 5 July 1967.
- 1.2 Pre-simulation Report LM Dynamic Simulation, Massachusetts Institute of Technology, Instrumentation Laboratory, E-2079, September 1966.
- 2.1 Directory of Standard Geodetic and Geophysical Constants for Gemini and Apollo, NASA General Working Paper No. 10, 020B, 6 April 1966.
- 2.2 Apollo Mission Data Specification "C" Apollo-Saturn 206A (U), TRW Systems, 2131-6002-TC000, 5 November 1965.
- 2.3 Undocumented estimate.
- 2.4 MIT Apollo Guidance and Navigation Information, Massachusetts Institute of Technology, Instrumentation Laboratory, G-532, 28 November 1962.
- 4.1 Lunar Excursion Module Primary Guidance Navigation and Control Subsystem Equipment Performance and Interface Specification, Grumman Aircraft Engineering Corporation, LSP 370-3, 18 March 1966.
- 4.2 Specific Station Locations of Coupled LEM/CSM, GN and C Data Exchange Submittal, S-36, 3 August 1966.
- 4.3 Vehicle Dynamics Equation for the Full Mission Engineering Simulator, Grumman Aircraft Engineering Corporation, LMO 500-258, 5 August 1965.
- 4.4 LM-3 Mass Properties Data, US Memorandum, PM3/M-215/67, 6 October 1967.
- 4.5 Master End-Item Specification for LM, Grumman Aircraft Engineering Corporation, LSP-470-2C, SCN 222A - 188, 6 July 1967.
- 4.6 Results of The Effects of RCS Thruster Plume Impingement on The LM-2 & LM-3 Descent Stage, Grumman Aircraft Engineering Corporation, LMO 310-385, 19 June 1968.

- 4.7 Revised Apollo Mission Data Specification (AMDS) "D" for AS-204 (LM-1), US Memorandum, PD7/M-278/67, 12 December 1967.
- 4.8 LM G and C Data Book, Revision 2, NAS 9-4810, 15 July 1967.
- 4.9 Effect of Gimballed Engine Mount Compliance, Grumman Aircraft Engineering Corporation, LAV 500-619, 1 August 1967.
- 4.10 Abort Stage Sequence of Events, Grumman Aircraft Engineering Corporation, LMO 500-441, 23 August 1966.
- 4.11 FITH (Fire-in-the-hole) Force and Moment Impulses for LM-1 Through LM-4 Abort-Stage Situations, Grumman Aircraft Engineering Corporation, LMO 500-530, 16 January 1967.
- 4.12 LM Descent Engine Phase B Qualification Test Performance, US Memorandum, 28 September 1967.
- 4.13 A Comparison Between a "Static" and "Dynamic" Liquid Propellant Method for Calculating LM Mass Properties, Grumman Aircraft Engineering Corporation, LMO 500-583, 1 June 1967.
- 4.14 Ascent Engine Thrust Location, GN&C Data Exchange Submittal, MSC-S-58, 1 November 1967.
- 4.15 Mission Modular Data Book, Grumman Aircraft Engineering Corporation, LED 500-19, 15 October 1967.
- 4.16 Private Communication, R. Portnoy, GAEC, to K. Glick, MIT/IL, 13 October 1967.
- 4.17 Private Communication, R.D. Baker, TRW Systems, to H. Chasan, MIT/IL, 16 February 1968.
- 4.18 Design Control Specification for Propulsion Subsystem, Grumman Aircraft Engineering Corporation, LSP 270-6B, 5 May 1967.
- 4.19 Startup and Shutdown Impulse of LM DE, TRW Systems, 4721.3.67-200, 10 August 1967.

- 4.20 Prelaunch Checkout of PGNCS Auto Descent Engine On/Off Control, Grumman Aircraft Engineering Corporation, LMO 500-522, 9 December 1966.
- 4.21 Shutdown Characteristics of the LM Descent Engine, TRW Systems, 4721.3.67-257, 19 October 1967.
- 4.22 Method of Checkout for Auto-PGNCS Descent Engine Gimbal Trim, Grumman Aircraft Engineering Corporation, LMO-500-456, 8 July 1966.
- 4.23 Prelaunch Checkout of PGNCS/AGNCS Auto Ascent Engine On/Off Control, Grumman Aircraft Engineering Corporation, LMO 500-474, 15 August 1966.
- 4.24 Determination of Valve Response Times for the Ascent Engine Control Solenoid Valves and Actuator Isolation Valves, Grumman Aircraft Engineering Corporation, LAV 540-530, 15 July 1966.
- 4.25 Evaluation of the LM DE Shallow Throttling Concept with Respect to a Lunar Landing Mission, TRW Systems, 4721.3.68-52, 27 February 1968.
- 4.30 CSM/LM Spacecraft Operational Data Book, Volume III, Mass Properties, Manned Spacecraft Center, SNA-8-D-027, March 1968.
- 4.31 SPS Propellant Sloshing Parameters, North American Aviation, FS/GCA/65-241, 15 September 1965.
- 4.32 GN&C Data Submittal, NAA-S-68, 11 March 1966.
- 4.33 CM 103 and LM 3 Mass Properties, GN&C Data Submittal, MSC-S-59, 14 November 1967.
- 4.34 Private Communication, R. Morton, MSC to H. Chasan, MIT/IL, 4 December 1967.
- 4.35 BLK II SPS Propellant by Tank, GN&C Data Submittal, MSC-S-62, 20 December 1967.
- 4.36 Three Dimensional Vibrational Modes of the Apollo CSM/LM Docked Vehicles, TRW Systems, 05952-H239-R0-00, 30 June 1967.

- 4.37 Dynamic Characteristics of the CSM/LM Docked Vehicle During LM DPS Burn, Manned Spacecraft Center, MSC-S-75, 22 May 1968.
- 4.38 CSM/LM Spacecraft Operational Data Book, Volume II, LM Data Book, Manned Spacecraft Center, SNA-8-D-027, June 1968.
- 4.39 Results of RCS Engine Supplemental Qualification Test Program, Grumman Aircraft Engineering Corporation, LMO-310-335, 14 March 1967.
- 4.40 PCR 587.2, APS and DPS Tail-off Constants, 29 October 1968.
- 4.41 Private Communication, H. Byington, MSC to T. Price, Jr., MSC, 25 October 1968.
- 5.1 Apollo Operations Handbook, Lunar Module, LM-3, Volume I, Grumman Aircraft Engineering Corporation, LMA-790-3-LM3, 1 January 1968.
- 5.2 Radar Section Study Guide, Lunar Module, LM-3, Grumman Aircraft Engineering Corporation, LSG 770-430-44-LM3, February 1968.
- 5.3 Primary Guidance Navigation and Control System to Rendezvous Radar Angle Electrical Interface Control Document, Grumman Aircraft Engineering Corporation, LIS 370-10006, 30 July 1965.
- 5.4 Block II Moding and Programming Requirements, Massachusetts Institute of Technology, Instrumentation Laboratory, Apollo Project Memo 1259, 20 April 1965.
- 5.5 LEM Seventh Quarterly Design Report, Rendezvous Radar/Transponder, Volume I of II, Radio Corporation of America, 15 September 1965.
- 5.6 Third Radar Design Review, Radio Corporation of America, 15 May 1968.
- 5.7 Lunar Excursion Module Primary Guidance Navigation and Control Subsystem Equipment Performance and Interface Specification, Grumman Aircraft Engineering Corporation, LSP 370-3, 18 March 1966.
- 6.1 Directory of Standard Geodetic and Geophysical Constants for Gemini and Apollo, NASA General Working Paper No. 10, 020B, 6 April 1966.



LUMINARY
Section 6

Internal:

P. Adler (2)	M. Johnston	R. Ragan
R. Battin	E. Jones	K. Riebesell
E. Blanchard	G. Kalan	R. Rose
H. Chasan	D. Keene	P. Rye
G. Cherry (3)	J. Kernan	J. Sapanaro
A. Cook	*J. Kingston	C. Schulenberg
E. Copps	A. Kosmala	N. Sears
S. Copps	G. Kossuth	A. Seidler
S. David	W. Kupfer	J. Shillingford
W. Day	A. Laats	L. Silver
J. Deckert	L. Larson	B. Sökkappa
G. Eddleston	R. Larson	W. Stameris
G. Edmonds	D. Lickly	R. Stengel
P. Felleman	R. Lones	R. Strunce
L. Gediman (20)	W. Marscher	G. Stubbs
J. Glendenning	F. Martin	J. Suomala
K. Glick	H. McOuat	J. Sutherland
K. Goodwin	R. Metzinger	W. Tanner
R. Goss	J. E. Miller	R. Tinkham
E. Grace	J. S. Miller	K. Vincent
K. Green	P. Mimno	J. Vittek
D. Gustavson	R. Morth	R. Weatherbee
P. Heinemann	J. Morse (2)	P. Weissman
J. Henize	E. Muller	J. Wells
J. Heybl	J. Nevins	C. Wenk
D. Hoag	J. O'Connor	R. Werner
B. Ireland	L. Petrillo	P. White
T. Isaacs	P. Philliou	W. Widnall
I. Johnson	P. Plender	M. Womble
L. B. Johnson (2)	P. Pu	C. Work
M. Johnson		Apollo Library (2)
		MIT/IL Library (6)

*Letter of Transmittal only.

NASA/RASPO GE	NASA Daytona Beach Operation P.O. Box 2500 Daytona Beach, Florida 32015 Attn: Mr. A. S. Lyman	(1)
NASA/HDQ	NASA Headquarters 600 Independence Avenue SW Washington, D.C. 20546 Attn: MAP-2 Attn: Mission Director, Code MA Attn: Robert Aller, Code MAO	(6) (4) (1) (1)
NASA/LEWIS	National Aeronautics and Space Administration Lewis Research Center Cleveland, Ohio Attn: Library	(2)
NASA/FRC	National Aeronautics and Space Administration Flight Research Center Edwards AFB, California Attn: Research Library	(1)
NASA/LRC	National Aeronautics and Space Administration Langley Research Center Langley AFB, Virginia Attn: Mr. A. T. Mattson	(2)
NASA/GSFC	National Aeronautics and Space Administration Goddard Space Flight Center Greenbelt, Maryland Attn: Mr. Paul Pashby, Code 813	(2)
GAEC	Grumman Aircraft Engineering Corporation Bethpage, Long Island, New York Attn: Mr. J. Marino Mr. C. Tillman Mr. F. Wood Mr. H. Sherman Mr. R. Pratt Mr. B. Sidor Mr. R. Kress	(23 + 1R) (1R) (13) (1) (3) (4) (1) (1)
NAR	North American Rockwell Inc. Space and Information Systems Division 12214 Lakewood Boulevard Downey, California 90241 Attn: Apollo Data Requirements Dept. 096-340 Building 3, CA 99	(1 + 1R)

NASA/RASPO GAEC	National Aeronautics and Space Administration Resident Apollo Spacecraft Program Officer Grumman Aircraft Engineering Corporation Bethpage, Long Island, New York	(1)
NASA/RASPO ACED	National Aeronautics and Space Administration Resident Apollo Spacecraft Program Officer AC Electronics Division General Motors Corporation Milwaukee, Wisconsin 53201 Attn: Mr. W. Swingle	(1)
NASA/WSMR:	National Aeronautics and Space Administration Post Office Drawer MM Las Cruces, New Mexico Attn: RH4 Documentation	(2)
NASA/MSFC:	National Aeronautics and Space Administration George C. Marshall Space Flight Center Huntsville, Alabama Attn: J. Mack R-ASTR-5 (1) H. Ledford R-AERO-P (2) L. McNair R-AERO-P (1) T. Telfer R-AERO-DA (2) E. Deaton R-AERO-DA (1) J. Cremin R-AERO-DAP (1) L. Stone R-AERO-F (1) C. Hagood R-AERO-F (1) O. Hardage R-AERO-FM (1) F. Moore R-ASTR-N (1) S. Seltzer R-ASTR-NG (5) H. Hosenthien R-ASTR-F (1) A. McNair I-MO-R (1) D. Germany I-I/IB-E (1) R. Barraza I-V-E (1) W. Chubb R-ASTR/NG (1) J. McCullough I-VE/T (1)	(23)
NASA/MSC	National Aeronautics and Space Administration Manned Spacecraft Center Apollo Document Control Group (PA 2) Houston, Texas 77058 Attn: A. Alber, FS5 (letter of transmittal only)	150 + 2R
BELLCOMM:	Bellcomm, Inc. 1100 17th Street N.W. Washington, D.C. 20036 Attn: Info. Analysis Section	(6)
LINK:	LINK Group, GPSI SIMCOM 1740 A NASA Boulevard Houston, Texas 77058 Attn: Mr. D. Klingbell	(3)
TRW:	Gilbert H. Friedman Building 82 Rm 2067 TRW System Group One Space Park Redondo Beach, California 90278	(5)